Evolution of turbulent spots in a parallel shear flow

Jörg Schumacher and Bruno Eckhardt
Fachbereich Physik, Philipps-Universität Marburg, D-35032 Marburg, Germany
(Received 25 February 2000; revised manuscript received 26 October 2000; published 27 March 2001)

The evolution of turbulent spots in a parallel shear flow is studied by means of full three-dimensional numerical simulations. The flow is bounded by free surfaces and driven by a volume force. Three regions in the spanwise spot cross section can be identified: a turbulent interior, an interface layer with prominent streamwise streaks and vortices, and a laminar exterior region with a large scale flow induced by the presence of the spot. The lift-up of streamwise streaks that is caused by non-normal amplification is clearly detected in the region adjacent to the spot interface. The spot can be characterized by an exponentially decaying front that moves with a speed different from that of the cross-stream outflow or the spanwise phase velocity of the streamwise roll pattern. Growth of the spots seems to be intimately connected to the large scale outside flow, for a turbulent ribbon extending across the box in the downstream direction does not show the large scale flow and does not grow. Quantitatively, the large scale flow induces a linear instability in the neighborhood of the spot, but the associated front velocity is too small to explain the spot spreading.

DOI: 10.1103/PhysRevE.63.046307 PACS number(s): 47.20.Ft, 47.27.Cn, 47.54.+r

I. INTRODUCTION

The transition to turbulence in spatially extended systems does not necessarily take place at all points simultaneously but can be preceded by the formation of localized structures that grow to eventually fill space. The first experiments by Reynolds on pipe flow already showed the formation of turbulent spots and slugs [1,2]. In Couette-Taylor flow between counter-rotating cylinders turbulence can be confined to propagating spirals [3,4]. Localized turbulence has also been observed in plane Couette flow [5] where the fraction of space filled with turbulent flow has been used as a measure to define the transition to turbulence [6–8]. Besides these transitional phenomena, localized turbulent spots can also be observed in high-Reynolds-number boundary layers [9].

It is tempting to connect both the localization of spots, i.e., the coexistence of laminar and turbulent phases of the shear flow, and the propagation of sharp boundaries, i.e., a frontlike structure, to phenomena studied in considerable detail within amplitude models [10]. Indeed, some models show qualitatively similar behavior. There are, however, several problems that raise questions about the applicability of such models. For instance, they are not derived from the Navier-Stokes equation and the extent to which they reflect the hydrodynamical processes and interactions remains an open question. Furthermore, amplitude equations work best if they can be applied in a situation of linear instability and small amplitudes [11], such as the onset of Rayleigh-Bénard convection near the critical point [12]. But many of the turbulent spots arise in shear flows that are linearly stable, at least in the Reynolds number region of interest here. Such behavior can be captured in higher-order Ginzburg-Landau models [13], but the required large amplitudes complicate a quantitative comparison. Moreover, investigations of plane Couette flow show that the turbulent state is not stable but can decay spontaneously for lower-Reynolds-number values [14–16].

It is our aim here to analyze the evolution of turbulent spots in parallel shear flows, in particular their spanwise spreading. Our flow has free-slip boundary conditions and is driven by a volume force. Despite the change in boundary conditions we observe features similar to those in experiments on plane Couette flow with rigid boundary conditions and a linear shear profile: this supports the expectation that there are perhaps universal aspects. The model is, moreover, well suited for high-resolution direct numerical simulations with a Fourier-pseudospectral method and allows for a detailed investigation of the dynamics in the transitional region. In particular, we focus on characterization of the front that separates the laminar and turbulent regions, on the mechanism by which it propagates, on the Reynolds number dependence of the front speed, and on the large scale flow in the laminar surroundings of the spot. As we will discuss in more detail in the appropriate sections these aspects complement previous numerical and experimental investigations in wall bounded shear flows [17–24].

The paper is arranged as follows. After introducing the physical model and the numerical procedures in Sec. II we discuss in Sec. III the hydrodynamics of the spreading mechanism in some detail. The properties of the tail of the envelope, such as spatial decay and spreading velocity, are discussed and three different regimes of the spreading process are identified. In Sec. IV we discuss the results and give a brief outlook.

II. THE MODEL

The system we consider here is a shear flow between parallel free-slip surfaces and driven by a volume force. In the streamwise and spanwise directions periodic boundary conditions are applied; in the normal direction the normal velocity component vanishes in the two bounding surfaces. With lengths measured in units of $d/2$ (half the gap width) the periodicities in streamwise and spanwise directions are both 80. The volume force with a sinusoidal dependence in the normal direction gives rise to a laminar profile with ve-

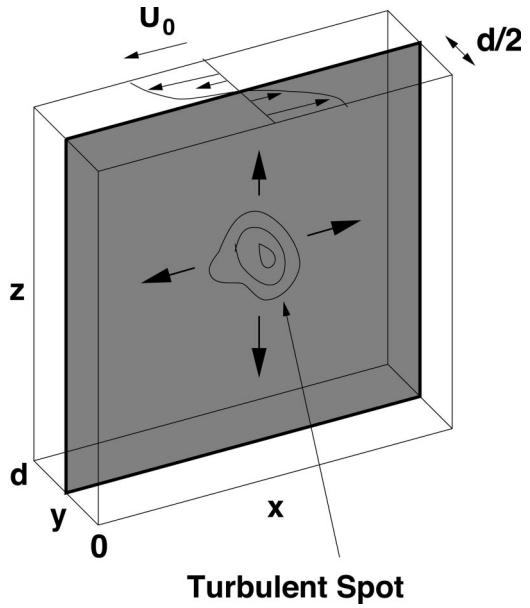

FIG. 1. Geometry of the flow. The x axis points in the streamwise, y in the wall-normal, and z in the spanwise direction. The central plane at $y=1$ in which the spreading is analyzed is shaded gray.

locities $\pm U_0$ at the surfaces. The Reynolds number is defined as $\mathrm{Re}=U_0 d/(2\nu)$. In these units the incompressible Navier-Stokes equation for a velocity field $\mathbf{u}(\mathbf{x},t)$ becomes

$$\frac{\partial \mathbf{u}}{\partial t}+(\mathbf{u}\cdot\boldsymbol{\nabla})\mathbf{u}=-\boldsymbol{\nabla}p+\frac{1}{\mathrm{Re}}\boldsymbol{\nabla}^2\mathbf{u}+\mathbf{f}, \tag{1}$$

$$\boldsymbol{\nabla}\cdot\mathbf{u}=0, \tag{2}$$

where $p(\mathbf{x},t)$ denotes the pressure and $\mathbf{f}(\mathbf{x},t)$ the external volume force specified below.

Figure 1 shows the Cartesian coordinate system we use, with x pointing in the streamwise, y in the wall-normal, and z in the spanwise direction. The fluid volume is confined to $0\leqslant y\leqslant 2$ with boundary conditions

$$u_y=\frac{\partial u_x}{\partial y}=\frac{\partial u_z}{\partial y}=0 \quad \text{at} \quad y=0 \quad \text{and} \quad 2 \tag{3}$$

at the surfaces and periodic boundary conditions in the downstream and spanwise directions.

The shear flow is driven by a volume force $\mathbf{f}=\pi^2/(4\,\mathrm{Re})\cos(\pi y/2)\mathbf{e}_x$ acting in the x direction, which in the laminar regime sustains a flow $\mathbf{U}_0=\cos(\pi y/2)\mathbf{e}_x$. The velocity field $\mathbf{u}(\mathbf{x},t)$ is decomposed into this laminar flow $\mathbf{U}_0$ and a turbulent part $\mathbf{v}(\mathbf{x},t)$. As shown already by Tollmien, $\mathbf{U}_0$ is linearly stable, thus demonstrating that Fjørtoft's theorem is a necessary but not sufficient condition for the transition to turbulence [25]. Nevertheless, for sufficiently large driving the flow shows a transition to turbulence.

The free-slip or stress-free boundary conditions have the advantage that the flow can be represented completely by Fourier modes so that robust pseudospectral techniques based on a 2/3-rule dealiasing and an adaptive Runge-Kutta scheme for advancing in time can be used [26,27]. To account for boundary conditions the flow is represented by the Fourier sums

$$u_x(\mathbf{x},t)=\sum_{\mathbf{k}} u_{x\mathbf{k}}(t)\cos(k_y y)\exp[i(k_x x+k_z z)], \tag{4}$$

$$u_y(\mathbf{x},t)=\sum_{\mathbf{k}} u_{y\mathbf{k}}(t)\sin(k_y y)\exp[i(k_x x+k_z z)], \tag{5}$$

$$u_z(\mathbf{x},t)=\sum_{\mathbf{k}} u_{z\mathbf{k}}(t)\cos(k_y y)\exp[i(k_x x+k_z z)] \tag{6}$$

with wave numbers

$$k_y=0,\frac{\pi}{2},\pi,\ldots,\frac{N_y\pi}{2}, \tag{7}$$

$$k_x=0,\pm\frac{2\pi}{L_x},\pm 2\frac{2\pi}{L_x},\ldots,\pm\frac{N_x}{2}\frac{2\pi}{L_x}, \tag{8}$$

$$k_z=0,\pm\frac{2\pi}{L_z},\pm 2\frac{2\pi}{L_z},\ldots,\pm\frac{N_z}{2}\frac{2\pi}{L_z}. \tag{9}$$

In [28] and [8], respectively, low-dimensional models for the transition to turbulence in plane shear flows with stress-free boundary conditions were discussed. Their basic flow has the form $U_{0x}(y)\sim\sin(\pi y/2)$ and is confined to an interval $y\in[-1,1]$. Both expansions can thus be related by a shift in the interval, but we prefer Eqs. (4)–(6) as it has the more compact representation in sines and cosines and is easier to implement numerically. The spectral resolution for all runs with evolving spots was $N_x\times N_y\times N_z=256\times 33\times 512$. The initial localized perturbation is a poloidal vortex of the form

$$\mathbf{v}(\mathbf{x},t=0)=\boldsymbol{\nabla}\times\boldsymbol{\nabla}\times A\exp[-a_x^2(x-x_0)^2 - a_y^2(y-y_0)^2-a_z^2(z-z_0)^2]\mathbf{e}_y, \tag{10}$$

positioned slightly off center in order to avoid spurious effects due to accidental symmetries. This initial condition is a model for the flow induced in experiments where a small transverse jet penetrates the laminar shear profile in the wall-normal direction [5–7].

For the analysis in the following sections we need the Reynolds number above which a transition to turbulence occurs. Because of the free-slip boundary conditions at the surface it can be expected to be below the one for rigid walls. But as in that case the transition is strongly intermittent and the best approach to a definition of a critical Reynolds number uses a statistical analysis of run time experiments with different initial conditions [29]. At each value of Re we run 30 trajectories starting from states with slightly different amplitudes A. The different initial conditions were obtained by switching on a field (10) with time-dependent amplitude $A(t)=a_0\sin^2(\pi t/2)$ for $t\in[0,2]$, where the factor a_0 was increased from 1.248 to 1.326 in steps of 0.0026. Since the aim is to obtain information on the bulk properties, we took

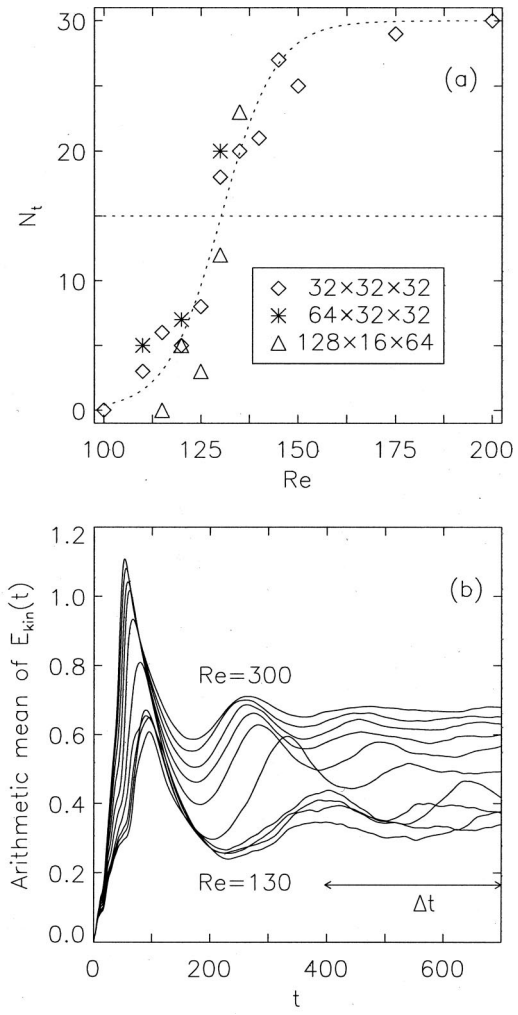

FIG. 2. Statistical analysis of the transition to turbulence. Panel (a) shows the number N_t of initial conditions that lead to persistent turbulence for different Reynolds numbers and for several spectral resolutions. 30 trajectories were run for every Reynolds number. The dashed line is a two-parameter least squares fit $N_t(\mathrm{Re}) = 15 \times \tanh[(\mathrm{Re} - A_0)/A_1] + 15$. Panel (b) shows the temporal relaxation of the turbulent kinetic energy, averaged over all trajectories that became turbulent. The double headed arrow marks the interval of temporal averaging used for Eq. (13).

a smaller box with aspect ratio $L_x:L_y:L_z = 40:2:20$ (in units of half the gap width), and a lower spectral resolution. As in the direct numerical simulations of plane Couette flow [29], two types of dynamics can be identified: in one case the flow builds up and the energy relaxes with oscillations to the turbulent state, i.e., $E_{kin} \neq 0$, whereas in the other case the state decays toward the laminar profile, so that finally E_{kin} becomes negligible. The number N_t of initial conditions that became turbulent vs Reynolds number is shown in panel (a) of Fig. 2. For $\mathrm{Re} \gtrsim 200$ all samples relax to the turbulent state and the turbulent energy increases linearly with Reynolds number, giving rise to the relation (13). As in the case of plane Couette flow, the relaxation to the turbulent state is oscillatory [Fig. 2(b)]. We conclude from these studies that more than half the initial conditions will become turbulent for Reynolds numbers of 130 ± 5, which, as expected, is lower than the value of 320 ± 10 for rigid boundary conditions [29]. Below this Reynolds number most turbulence is transient and a turbulent region can disappear by erosion from within. Thus, the kind of spot spreading phenomenon we are interested can occur only for Reynolds numbers above this value.

III. SPREADING OF THE TURBULENT SPOT

After a short transient of about 5 time units the inital perturbation which was localized in diameter to about 4 half gap width units develops streamwise streaks and vortices and starts to expand. To highlight the turbulent deviations about the laminar flow a contour plot of the downstream velocity averaged over half a box height,

$$\overline{v_x}(x,z,t) = \int_0^1 v_x(x,y,z,t)\,dy, \tag{11}$$

is shown in Fig. 3 (left panel). The elongated streamwise streaks with alternating flow direction stand out above the background flow. The cut at $x = L_x/2 = 40$ for the streamwise turbulent velocity itself underlines the existence of the streamwise streaks (right panel). In the streamwise direction the spot advances more or less stochastically, with the unpredictable appearance of turbulent bursts which are then advected by the laminar profile. This causes a strongly fragmented spot interface. In the spanwise direction it advances more steadily with a regular interface and it is this direction we focus on in the following analysis.

Cross sections of the local turbulent energy $\mathbf{v}^2$ taken in the middle of the cell at $x = L_x/2$ and $y = 1$ for fixed time indicate three different flow regimes: a turbulent interior, a laminar exterior, and a narrow transitional region with large velocity amplitudes and a rather regular spatial structure (see Fig. 4). We will discuss these regions in turn.

A. Turbulent interior and wave propagation at the spot interface

The turbulent fluctuations in the interior were investigated in detail for five values of the Reynolds number, as shown in

TABLE I. Characteristic velocities of the spreading spot in units of U_0 for several Reynolds numbers: the phase velocity v_w, the front velocity v_F, and the root mean square velocities of the three components v_i with $i = x, y$, and z. The phase velocity was determined separately for the maxima and minima of v_x closest to the boundary and their arithmetic mean is listed. The turbulent fluctuations taken over a small volume in the spot center were in addition averaged over time between $t = 30$ and 50. The third column is the root mean square velocity $(\langle v_x^2 \rangle + \langle v_y^2 \rangle + \langle v_z^2 \rangle)^{1/2}$.

Re	v_w	v_F	$\sqrt{\langle v^2 \rangle}$	$\sqrt{\langle v_x^2 \rangle}$	$\sqrt{\langle v_y^2 \rangle}$	$\sqrt{\langle v_z^2 \rangle}$
150	0.02	0.09	0.19	0.18	0.02	0.05
200	0.08	0.42	0.41	0.38	0.09	0.12
250	0.14	0.56	0.50	0.45	0.13	0.19
300	0.17	0.63	0.61	0.56	0.15	0.19
350	0.16	0.64	0.57	0.53	0.13	0.19

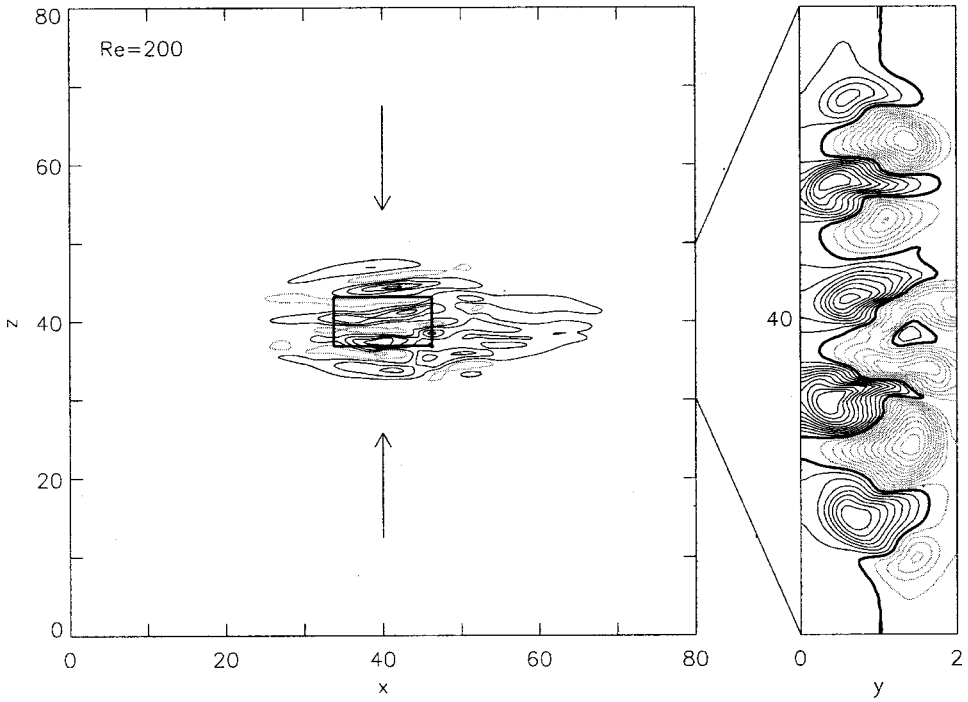

FIG. 3. Streamwise streaks in an expanding spot for Re=200 at $t=39$. Left: Contours of $\overline{v_x}(x,z)$. The rectangular box in the spot center marks the lateral extension of the volume used for the analysis of internal turbulent fluctuations. Right: Magnification of the wall-normal–spanwise plane at $x=L_x/2$ (marked by arrows in the left panel). Corresponding contours of $v_x(x=L_x/2,y,z)$ are plotted using the same line style: gray lines denote negative values, black lines positive ones, and the heavy solid line is $v_x=0$.

Table. I. The fluctuations, in units of U_0^2, were obtained by averaging over a box V_c of size $l_x:l_y:l_z=12:2:6$ (see the left panel of Fig. 3) in the center of the spot according to

$$\langle v_i^2\rangle(t_0)=\frac{1}{V_c}\int_{V_c} v_i^2(x,y,z,t_0)dV \quad \text{for} \quad i=x,y,z. \quad (12)$$

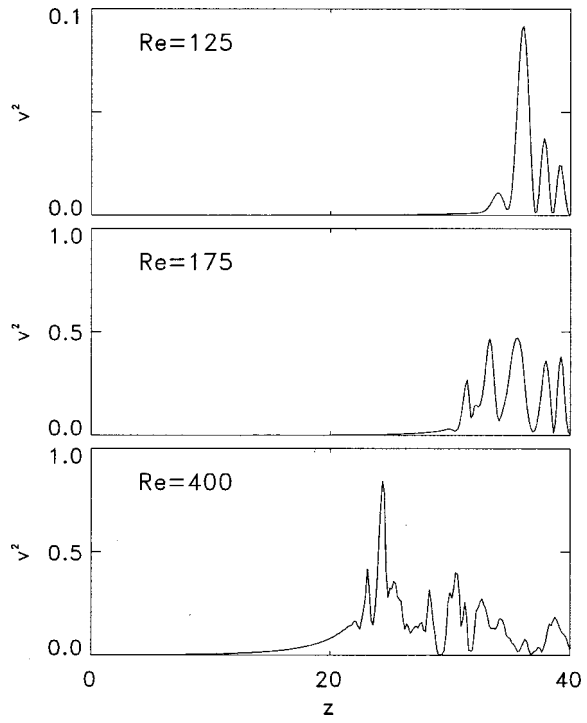

FIG. 4. Envelopes of the turbulent kinetic energy along the spanwise axis for three different Reynolds numbers at $t=59$ after inducing the perturbation.

For a Reynolds number of about 150, where the spot decays, the fluctuations decrease with time. For higher Reynolds numbers they first increase until a time of about 30 and then stay constant, within statistical fluctuations. The values quoted in the table are the temporal averages taken between $t=30$ and 50. As expected, the streamwise fluctuations are largest but smaller than the fluctuations in the interface region (see Fig. 4).

The spatial modulations near the interface are due to elongated streamwise structures, so-called streamwise streaks, which are not stable but travel slowly in the spanwise direction with a phase velocity v_w. The occurrence of such (oblique) waves was noted in several previous investigations, mainly for plane Poiseuille flow, and has been connected to an inflectional instability of the combined shear and cross flow velocity field [17,21]. A linear stability analysis of the combined profile for plane Poiseuille and plane Couette flow gives a range of critical wave numbers (see [18,20] and below).

The spreading of the spot in the spanwise direction is further documented in Fig. 5 for Re=200. The streamwise vorticity component $\omega_x=\partial_y v_z-\partial_z v_y$ is shown in the upper panels. The growth of a pair of new counter-rotating vortices (panel numbers 2, 3, and 4 of Fig. 5) can be followed for all eight snapshots. The corresponding streamwise streak which is lifted up by the non-normal amplification can also be identified in the cross section of the streamwise velocity v_x (see the lower panels). Although there is a certain discreteness in the growth of new streamwise rolls and pairs of streamwise vortices, the front advances steadily in time without any disruptions, as will be shown later in Sec. III C.

In Table I we have included the results for the phase velocity v_w of the streaks. The wavelength was also determined as the distance between two streaks with the same

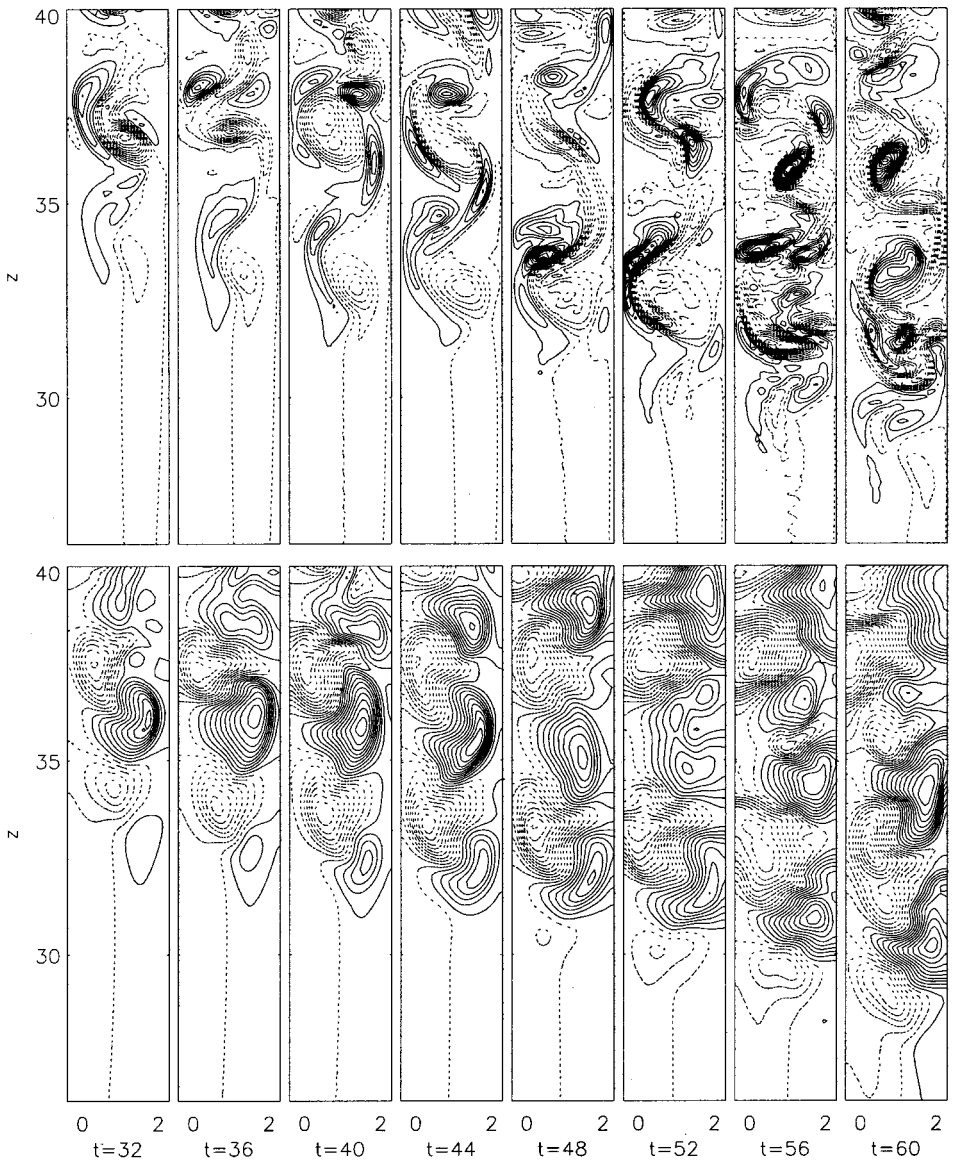

FIG. 5. Snapshots of the streamwise vorticity ω_x (upper row) and the streamwise velocity v_x (lower row). The data are for Re=200 at $x=L_x/2=40$. Dotted lines denote positive contours and solid lines negative ones. Horizontal axis denotes wall-normal direction in all panels.

sign, i.e., the spatial distance between two maxima or minima of v_x, measured in units of $d/2$. We found values between 2.4 and 3.4 with a tendency toward smaller values for higher Re. Velocities were determined by monitoring the motion of these maxima and minima in v_x. Only extrema closest to the interface were included and measurements were limited to times between $t=32$ and $t=60$ for all five data sets. We find that the phase speed increases with Reynolds number.

B. The large scale flow outside the spot

Near the spanwise centerline across the spot we find a strong outward pointing flow. It varies with height but is not compensated by an inflow on any level. Incompressibility thus demands a compensating inflow in other parts of the spot. The magnitude of this large scale flow decreases rather rapidly with distance from the spot and accounts almost completely for the deviations from the laminar profile. In order to highlight the flow pattern we show in Fig. 6 the directional field, i.e., $\overline{\mathbf{v}}/|\overline{\mathbf{v}}|$, where the overbar indicates an average in the normal direction. The flow has quadrupolar characteristics, with outflow in the spanwise direction and inflow in the streamwise direction.

The outward velocity does not coincide with the phase speed of the waves. But, small as the large scale flow may be, it has profound consequences for the spreading of the spot. Consider, for instance, the case of a ribbon spanning the periodicity box in the streamwise direction but localized in the spanwise direction: no such quadrupolar flow can form. And, indeed, the ribbon does not spread [see the dashed line in panel (a) of Fig. 9 below].

C. The propagating front

Outside the spot and into the laminar regime one notes a gradual decrease in local turbulent energy $\mathbf{v}^2(\mathbf{x},t)$.

Quantitatively, the energy density decays exponentially, as demonstrated in Fig. 7, where segments of the turbulent spot envelopes of the lower front (moving toward $z=0$) be-

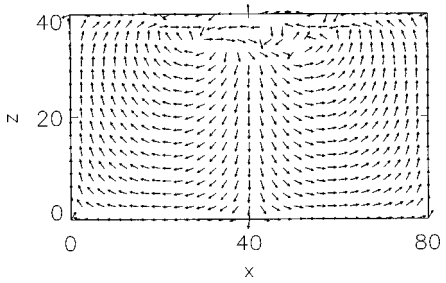

FIG. 6. Large scale flow outside the spot. To emphasize the topology of the flow field only the direction $\overline{\mathbf{v}}/|\overline{\mathbf{v}}|$, averaged in the wall-normal direction x, is shown. The domain is the lower half of the full integration domain, with the center of the spot in the middle of the upper boundary. The flow is for a Reynolds number of Re $=200$ at a time $t=39$.

tween $t=34$ and $t=50$ are plotted. The rate of spatial decay λ grows slowly for Reynolds numbers Re$\geqslant$200. By fitting to each of 11 snapshots separately an exponential profile $\sim\exp(-z/\lambda)$ gives decay rates λ between 0.9 and 1.2. In Fig. 8 the arithmetic mean and the corresponding error bars are shown for Re$\geqslant$175. For smaller Reynolds numbers deviations from an exponential envelope are larger, resulting in larger variations and uncertainties in the spatial decay rates. This exponentially decaying envelope is not much influenced by the turbulent fluctuations inside the spot and advances more or less steadily into the laminar region. Monitoring the position of a certain turbulent intensity threshold allows one to extract a velocity v_F that is independent of the selected threshold along the tail. However, since the turbulent intensity increases with Reynolds number it is advisable for numerical reasons to adjust the threshold also. We choose to increase the level linearly with Re,

$$\mathbf{v}^2=7.5\times10^{-3}\times[a_1+a_2(\mathrm{Re}-\mathrm{Re}_0)], \tag{13}$$

where the coefficients $a_1=0.143$, $a_2=2.6\times10^{-4}$, and $\mathrm{Re}_0=200$ follow from a linear fit to the mean kinetic energy $E_{kin}(t)=(1/2V)\int_V\mathbf{v}(\mathbf{x},t)^2dV$ as a function of Re. This variation of mean kinetic energy was determined alongside the statistical analysis needed to determine the Reynolds number for the transition to the turbulent state (see Sec. II).

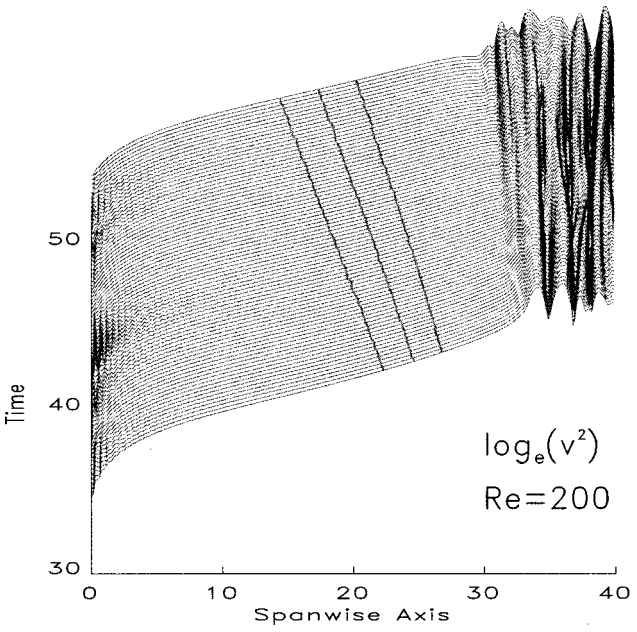

FIG. 7. The exponential decay toward the laminar profile outside the turbulent spot at Re$=$200. Shown are the profiles of the turbulent kinetic energy along the lower half of the center line on a semilogarithmic scale. Curves for different times in [34,50] are vertically displaced and overlayed. The lines across the plot indicate the motion of the levels at which the front velocity was determined.

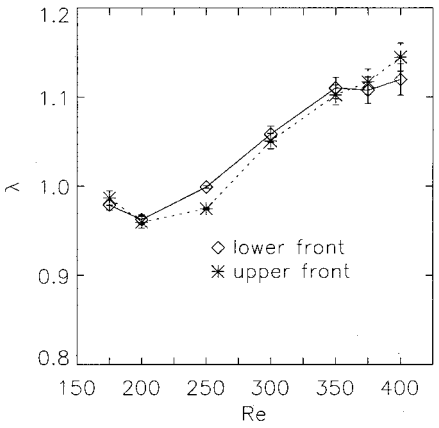

FIG. 8. Exponential decay rate λ of the envelope. The data are mean values taken from front envelopes as shown in Fig. 7.

The front speed thus determined is shown in panel (b) of Fig. 9. It increases for Reynolds numbers between 135 and 200 and saturates for Reynolds numbers above 300. Both regimes were also found in plane Couette flow experiments with rigid walls. Dauchot and Daviaud [22] observed an increasing spreading rate for Re between 370 and 450. Tillmark and Alfredsson found a constant spreading rate for Re$\gtrsim$500 [5]. In our simulations we can cover both ranges. Note that for Re$\leqslant$135 the velocity is negative, i.e., the spot shrinks rather than expands. This regime is difficult to detect numerically since at these Reynolds numbers the turbulence is not very stable and can decay spontaneously. This corresponds to an erosion of the spot from the inside. However, inspection of the flow field shows that in the time interval followed here the velocity given is connected with a retreating front and not an eroding spot [see also the innermost curves for the smallest Reynolds numbers in Fig. 9(a)]. As already mentioned in Sec. III A the spreading is monotonic in time as demonstrated by the curves in Fig. 9(a).

The Reynolds number at which the spots start to grow was used by Lundbladh and Johansson [19] as a definition for the threshold to turbulent behavior. Here we find that the spot starts to grow for Re$\simeq$135, a value compatible with the one determined by the statistical analysis in Sec. II, so that the results are consistent with [19].

D. The propagation mechanism

By now we have identified three velocities near the boundary of the turbulent spot: the front velocity v_F with

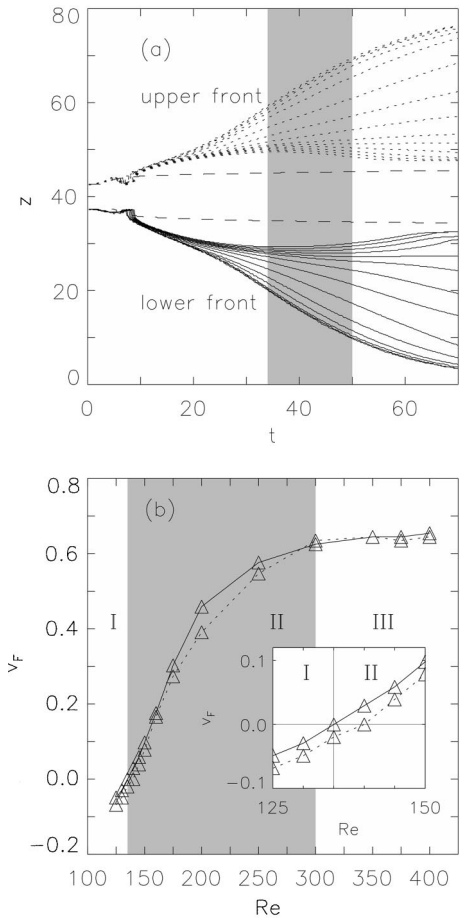

FIG. 9. Reynolds number dependence of the front velocity. (a) Position of the extracted level $\mathbf{v}^2$ of the envelope along the spanwise center line $(x=40,y=0,z)$ vs time t for both spanwise fronts. The outermost curves for the lower and upper fronts are taken at Re=400, the inner ones at Re=125. The dashed lines correspond to a run at Re=200 with a turbulent ribbon that extended across the box in the downstream direction. (b) Corresponding front velocities v_F (absolute values) extracted within the shaded time interval in panel (a). The inset highlights the crossover to the shrinking regime around Re$\simeq$135.

which the exponentially decaying part of the envelope propagates, the velocity of the spanwise outflow U_z, and the phase velocity v_w of the streamwise roll pattern. The value for U_z depends on the distance from the spot, but, even when calculated at the position of the first maximum of the turbulent fluctuations (see, e.g., Fig. 4), the value is smaller than the front speed v_F. Figure 5 shows that the outwards traveling roll patterns are eventually overtaken by the turbulent interior since v_F is larger than v_w.

In the absence of a linear instability of the laminar shear flow two possibilities for the growth mechanism have to be considered: a linear instability induced by the cross flow [9,17,18,22] and non-normal amplification [30–33].

The combination of basic profile and cross flow defines a rather steady laminar flow with stability characteristics different from those of the laminar profile. In the case of plane Poiseuille flow, Henningson could show that the combined flow is linearly unstable, but the front velocities deduced from this instability were smaller than the observed spreading velocity [17,18]. A complete stability analysis would have to include the full profile of the cross flow. An estimate of the expected spot growth rates may be based on a local approximation, where the values of the cross flow are kept fixed. We thus determine for each point z_0 along the spanwise centerline the cross flow

$$U_z(y,z_0)=U_z(0,z_0)+\frac{U_z(1,z_0)-U_z(0,z_0)}{2}[1-\cos(\pi y)], \tag{14}$$

where $U_z(0,z_0)\simeq U_z(2,z_0)$, and analyze the stability against perturbations

$$v_y(x,y,z,t)=\hat{v}_y(y)\exp[i(k_x x+k_z z-\omega t)], \tag{15}$$

where $\omega=\omega_r+i\tilde{\epsilon}$ is a complex frequency. This leads to the Orr-Sommerfeld equation

$$i\omega(D^2-k^2)\hat{v}_y+(ik_xU''_{0x}+ik_zU''_z)\hat{v}_y+\mathrm{Re}^{-1}(D^2-k^2)^2\hat{v}_y$$
$$-(ik_xU_{0x}+ik_zU_z)(D^2-k^2)\hat{v}_y=0, \tag{16}$$

with boundary conditions

$$\hat{v}_y(y)=\hat{v}''_y(y)=0 \quad \text{at} \quad y=0 \quad \text{and} \quad 2. \tag{17}$$

Here, $k^2=k_x^2+k_z^2$. The primes on the basic profiles U and D denote derivatives with respect to the wall-normal coordinate y. The local approximation is now reflected in the fact that the perturbations can have a z dependence, but the basic profile around which the perturbations are analyzed does not. With the form of the cross flow profile and a Fourier expansion for $\hat{v}_y(y)$ the Orr-Sommerfeld equation can be solved algebraically. The maximal growth rates $\epsilon=\max(\tilde{\epsilon})$ thus obtained are shown in Fig. 10 for points along the spanwise half-axis and for two values of the Reynolds number. For the lower value no linear instability is detected. For Reynolds numbers Re$\gtrsim$200 the local growth rate becomes positive, indicating a linear instability.

Investigations of other front-propagation problems, usually within a Ginzburg-Landau model, show that it is not only the local instability that determines the front speed but that the local curvature in wave number space has to be included as well. In the absence of a derivation of an amplitude equation in a turbulent medium we phenomenologically take the amplitude in the Ginzburg-Landau equation to model the envelope of the turbulent intensity $v^2(z,t)$, calculated in the middle of the cell at $x=L_x/2$ and $y=1$. The front then connects a laminar state $(A\simeq 0)$ with a turbulent one $(A\neq 0)$ [11,13]. For all practical purposes the turbulent state is stable and the laminar one, composed of the basic profile and the cross flow, shows a linear instability. Thus the simplest Ginzburg-Landau model with cubic nonlinearity should be appropriate,

$$\partial_t A=\epsilon A+D\partial_z^2 A-b_3A^3. \tag{18}$$

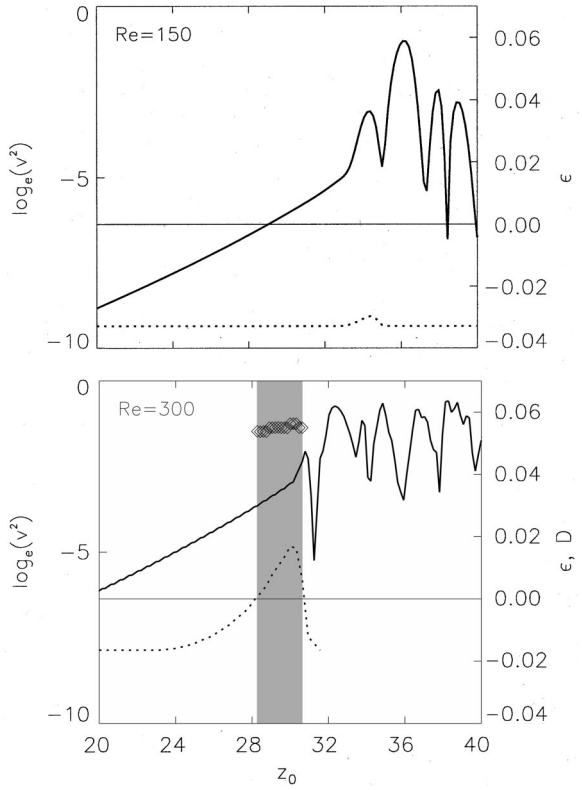

FIG. 10. Maximum growth rates ϵ of plane waves perturbing the mean flow combined with the cross-stream outflow along the spanwise axis. The sets for two different Reynolds numbers are compared at $t=39$. Thick solid lines denote $\log_e(v^2)$ and thick dotted lines denote maximum growth rate ϵ. Additionally, for Re=300 the diffusion coefficient D, which follows from the dispersion relation, is plotted for the gray shaded range of z_0 values.

The assumption is that the three parameters $\epsilon, D>0$ and $b_3>0$ are real. The marginal stability hypothesis then predicts a value for the asymptotic front velocity of

$$v^*=2\sqrt{\epsilon D}. \tag{19}$$

When taking the maximum growth rate ϵ of our data and evaluating the diffusion coefficient D by a saddle point approximation around the maximum of the dispersion relation $\omega=\omega(k_x,k_z)$, we end up with a front velocity that is about an order of magnitude smaller than the observed one. Corresponding to Eq. (19), one gets, e.g., $v^*\simeq 0.06$ for $\epsilon \simeq 0.017$, $D\simeq 0.056$, and Re=300 (see Fig. 10). However, at this Reynolds number the front moves with $v_F\simeq 0.63$.

This analysis of the front-propagation mechanism, with a local approximation, only cubic terms in the amplitude model, and without a discussion of slow transients [34] that could arise in such models, is rather simplified and can give only an indication of the expected front velocity. Nevertheless, it seems to us that even when these improvements are included the model cannot account for the observed spot spreading rates. First of all, it cannot say anything about the dynamics below a Reynolds number of about 200, where the spot spreads but where there is no instability. And, secondly, even above this Reynolds number, where there is a linear instability, the calculated front speed differs significantly from the observed one.

Besides the linear instability mode for spot growth there is another possibilty, based on the non-normal amplification of perturbations near the spot interface. Because of the action of the perturbation on the basic profile, streamwise vortices need not decay monotonically but can first grow on a time scale of order Re to an amplitude about a factor Re larger than the initial amplitude. This so-called lift-up effect [30] is most likely responsible for the occurence of streamwise streaks in turbulent shear flows where longitudinal modulations can give rise to secondary instabilities and a perpetual nonperiodic time evolution [16,33]. Indeed, we do observe this cyclic reproduction of the coherent structures in the interface region of the spot as demonstrated in the sequence of Fig. 5. The model then is that the turbulent interior of the spot induces a small perturbation near the interface which will then be amplified and grow turbulent. The statistical analysis of section II shows that not all perturbations grow turbulent. Thus, if most of the perturbations grow turbulent, the spot will spread, but if most of the perturbations decay, it will shrink. The observed coincidence between the critical Reynolds number for transition and the one for spot growth can be explained naturally in this picture. However, we do not see how to derive other quantitative conclusions from this model. In particular, the front speed would be given as the quotient of the width of the rolls generated (this can be read off rather accurately from the frames) and the time a perturbation needs to grow turbulent. The latter depends on the amplitude of the initial seed, the threshold for the transition to turbulence, and the amplification rate, none of which seems accessible to independent determination.

IV. FINAL REMARKS

Our analysis of a shear flow with free-slip boundary conditions on two parallel surfaces has revealed many similarities to plane Couette flow between rigid walls. As in that case three velocities connected with the spot can be identified, the velocities of the advancing front, of the outward flow component, and of the phase speed of (oblique) waves. They differ in value and in Re dependence, and relations between them are unknown. The dependence of the front velocity on the Reynolds number is consistent with experimental findings [5,22]. Many of the results reported here parallel the ones for plane Poiseuille flow. We also find waves and instabilities in the neighborhood of the spot, but they do not lead to quantitative predictions for the front velocity.

The conclusions we draw from this investigation highlight a dilemma. On the one hand, the large scale flow outside the spot does not seem to be important: the spot grows independent of whether there is a linear instability of basic flow plus large scale exterior flow or not, and if there is a linear instability the derived front speed is slower than the observed one. Moreover, the behavior expected from the non-normal amplification mechanism can explain some aspects of the dynamics, especially for lower Reynolds numbers. On the

other hand, if the outflow is suppressed, as in the case of a turbulent ribbon that spans the cell in the streamwise direction, no growth is observed despite the random initialization of seeds near the spot interface. Perhaps this can explain the observed stopping of growth in some experiments [22]. So it seems that spot growth is a subtle interplay between local features (e.g., non-normal amplification) and global features (such as the external flow). The connection between the two and a quantitative estimate of the growth velocity remain major puzzles in the dynamics of turbulent spots in parallel shear flows.

We thank Paul Manneville for discussions and the John-von-Neumann Institut für Computing in Jülich for computing time on a Cray T-90, without which this study would not have been possible.

[1] O. Reynolds, Proc. R. Soc. London **35**, 84 (1883).
[2] I. J. Wygnanski and F. H. Champagne, J. Fluid Mech. **59**, 281 (1973).
[3] D. Coles, J. Fluid Mech. **21**, 385 (1965).
[4] J. J. Hegseth, C. D. Andereck, F. Hayot, and Y. Pomeau, Phys. Rev. Lett. **62**, 257 (1989).
[5] N. Tillmark and P. H. Alfredsson, J. Fluid Mech. **235**, 89 (1992).
[6] F. Daviaud, J. J. Hegseth, and P. Bergé, Phys. Rev. Lett. **69**, 2511 (1992).
[7] S. Bottin, F. Daviaud, P. Manneville, and O. Dauchot, Europhys. Lett. **43**, 171 (1998).
[8] P. Manneville and O. Dauchot (unpublished).
[9] M. Gad-El-Hak, R. F. Blackwelder, and J. J. Riley, J. Fluid Mech. **10**, 73 (1981).
[10] M. C. Cross and P. C. Hohenberg, Rev. Mod. Phys. **65**, 851 (1992).
[11] Y. Pomeau, Physica D **23**, 1 (1986); **51**, 546 (1991).
[12] M. C. Cross, Phys. Fluids **23**, 1727 (1980).
[13] W. van Saarloos and P. C. Hohenberg, Physica D **56**, 303 (1992).
[14] A. Schmiegel and B. Eckhardt, Phys. Rev. Lett. **79**, 5250 (1997).
[15] A. Schmiegel and B. Eckhardt, Europhys. Lett. **51**, 395 (2000).
[16] S. Grossmann, Rev. Mod. Phys. **72**, 603 (2000).
[17] D. S. Henningson and P. H. Alfredsson, J. Fluid Mech. **178**, 405 (1987).
[18] D. S. Henningson, Phys. Fluids A **1**, 1876 (1989).
[19] A. Lundbladh and A. V. Johansson, J. Fluid Mech. **229**, 499 (1991).
[20] A. Lundbladh, Ph.D. thesis, Royal Institute of Technology, Stockholm, 1993.
[21] N. Tillmark, Europhys. Lett. **32**, 481 (1995).
[22] O. Dauchot and F. Daviaud, Phys. Fluids **7**, 342 (1995).
[23] S. Malerud, K. J. Måløy, and W. I. Goldburg, Phys. Fluids **7**, 1949 (1995).
[24] J. J. Hegseth, Phys. Rev. E **54**, 4915 (1996).
[25] P. G. Drazin and W. H. Reid, *Hydrodynamic Stability* (Cambridge University Press, Cambridge, 1981).
[26] C. Canuto, M. Y. Hussaini, A. Quaternioni, and T. A. Zang, *Spectral Methods in Fluid Dynamics* (Springer, Berlin, 1988).
[27] N. Seehafer, E. Zienicke, and F. Feudel, Phys. Rev. E **54**, 2863 (1996).
[28] F. Waleffe, Phys. Fluids **9**, 883 (1997).
[29] A. Schmiegel and B. Eckhardt (unpublished).
[30] M. T. Landahl, SIAM J. Appl. Math. **28**, 735 (1975).
[31] B. F. Farrell, Phys. Fluids **31**, 2093 (1988).
[32] K. M. Butler and B. F. Farrell, Phys. Fluids A **4**, 1637 (1992).
[33] F. Waleffe, Stud. Appl. Math. **95**, 319 (1995).
[34] U. Ebert and W. van Saarloos, Physica D **146**, 1 (2000).